Journal of Organometallic Chemistry 695 (2010) 707–716

Contents lists available at ScienceDirect

Journal of Organometallic Chemistry

journal homepage: www.elsevier.com/locate/jorganchem

Spectral, structural and DFT studies of platinum group metal 3,6-bis(2-pyridyl)-4-phenylpyridazine complexes and their ligand bonding modes

Kota Thirumala Prasad [a], Gajendra Gupta [a], A.K. Chandra [a], M. Phani Pavan [b], Kollipara Mohan Rao [a,*]

[a] Department of Chemistry, North Eastern Hill University, Shillong 793 022, India
[b] Department of Chemistry, University of Hyderabad, Hyderabad, India

ARTICLE INFO

Article history:
Received 18 November 2009
Received in revised form 2 December 2009
Accepted 8 December 2009
Available online 13 December 2009

Keywords:
Arene ligands
Pyridazine ligand
Platinum group metals
Ligand bonding modes
Density functional calculations

ABSTRACT

Reactions of 3,6-bis(2-pyridyl)-4-phenylpyridazine (L^{ph}) with $[(\eta^6\text{-arene})Ru(\mu\text{-Cl})Cl]_2$ (arene = C_6H_6, $p\text{-}^iPrC_6H_4Me$ and C_6Me_6), $[(\eta^5\text{-}C_5Me_5)M(\mu\text{-Cl})Cl]_2$, (M = Rh and Ir) and $[(\eta^5\text{-Cp})Ru(PPh_3)_2Cl]$ (Cp = C_5H_5, C_5Me_5 and C_9H_7) afford mononuclear complexes of the type $[(\eta^6\text{-arene})Ru(L^{ph})Cl]PF_6$, $[(\eta^5\text{-}C_5Me_5)M(L^{ph})Cl]PF_6$ and $[(Cp)Ru(L^{ph})(PPh_3)]PF_6$ with different structural motifs depending on the π-acidity of the ligand, electronic properties of the central metal atom and nature of the co-ligands. Complexes $[(\eta^6\text{-}C_6H_6)Ru(L^{ph})Cl]PF_6$ **1**, $[(\eta^6\text{-}p\text{-}^iPrC_6H_4Me)Ru(L^{ph})Cl]PF_6$ **2**, $[(\eta^5\text{-}C_5Me_5)Ir(L^{ph})Cl]PF_6$ **5**, $[(\eta^5\text{-Cp})Ru(PPh_3)(L^{ph})]PF_6$, (Cp = C_5H_5, **6**; C_5Me_5, **7**; C_9H_7, **8**) show the *type-A* binding mode (see text), while complexes $[(\eta^6\text{-}C_6Me_6)Ru(L^{ph})Cl]PF_6$ **3** and $[(\eta^5\text{-}C_5Me_5)Rh(L^{ph})Cl]PF_6$ **4** show the *type-B* binding mode (see text). These differences reflect the more electron-rich character of the $[(\eta^6\text{-}C_6Me_6)Ru(\mu\text{-Cl})Cl]_2$ and $[(\eta^5\text{-}C_5Me_5)Rh(\mu\text{-Cl})Cl]_2$ complexes compared to the other starting precursor complexes. Binding modes of the ligand L^{ph} are determined by ^1H NMR spectroscopy, single-crystal X-ray analysis as well as evidence obtained from the solid-state structures and corroborated by density functional theory calculations. From the systems studied here, it is concluded that the electron density on the central metal atom of these complexes plays an important role in deciding the ligand binding sites.

© 2009 Elsevier B.V. All rights reserved.

1. Introduction

Polypyridyl complexes of platinum group metals are being continuously investigated because of their multiple applications in fields of science including photophysics and photochemistry [1–6], supramolecular chemistry [7], catalysis [8–13] and bioinorganic chemistry [14–19]. The organometallic complexes of η^6-arene ruthenium [20,21] and η^5-half-sandwich complexes of rhodium and iridium have attracted considerable current interest as potential anticancer agents (Dyson et al.) [14–19,22,23]. Another important aspect, especially from the catalytic prospective, is the design of Ru=O functional groups and analogues capable of reversibly accepting multiple electrons and protons within a relatively small potential range [24–26]. This capacity to modify the environment in order to induce electronic as well as steric effects gives scope for the design and fabrication of tailored catalysts for specific reactions.

The properties of metal complexes largely depend on how the nature of the bridging ligand mediates metal–metal interactions. This role of bridging ligands is strongly influenced by factors such as the acceptor and donor properties of coordination sites, the length and rigidity of the spacers, the presence or absence of conjugated bonds, the orientation of substituents and the scope for manipulating ligand charge. In this regard, bridging polypyridyl ligands (*viz.* 2,2′-bipyrimidine (bpym), 2,3-bis(2-pyridyl)pyrazine (bppz), 3,5-bis(2-pyridyl)-1,2,4,5-tetrazine (bptz), 3,6-bis(2-pyridyl)pyridazine (bppn), and 2,4,6-tris(2-pyridyl)-1,3,5-triazine ligands) have received much attention [27–33]. The wider family of such ligands with 4- or 4,5-substituted pyridazine moieties (*viz.*, 3,6-bis(2-pyridyl)-4-phenylpyridazine (L^{ph}) (Fig. 1) has been relatively less studied. More recently, Constable and co-workers published a few reports on silver(I) complexes [34–37] incorporating such ligands.

Symmetrical 3,5-bis(2-pyridyl)-1,2,4,5-tetrazine (bptz) and to a lesser extent 3,6-bis(2-pyridyl)pyridazine (bppn) frequently bind *via* any two of the four nitrogen atoms present (N1 and N2 or N3 and N4) on the pyridine and tetrazine/pyridazine moieties, employing a bidentate κ^2 bonding mode to coordinate with d^6 metal centers [38,39]. A phenyl substituent introduces a element of asymmetry in the 3,6-bis(2-pyridyl)pyridazine (L) ligand moiety, as shown by the 3,6-bis(2-pyridyl)-4-phenylpyridazine (L^{ph}) ligand. This can bind to a metal *via* atoms N1 and N2 (*type-A*) or atoms N3 and N4 (*type-B*) (see Fig. 2) in a bidentate κ^2 bonding mode. The ligand is a four electron donor since the phenyl substituent creates differences in the electronic environment on the two available binding sites. Apart from the above two possibilities (*type-A* or *type-B*) (Fig. 2), a combination of the two types

* Corresponding author. Tel.: +91 364 272 2620; fax: +91 364 272 1010.
E-mail address: mohanrao59@gmail.com (K. Mohan Rao).

0022-328X/$ - see front matter © 2009 Elsevier B.V. All rights reserved.
doi:10.1016/j.jorganchem.2009.12.004

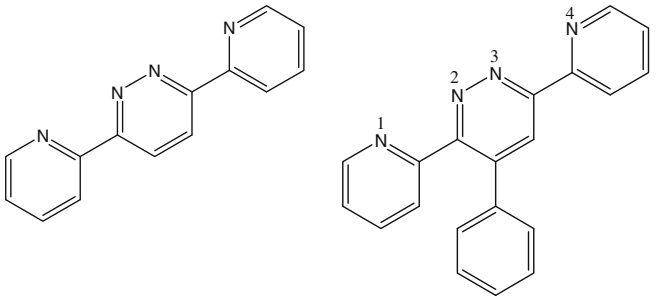

Fig. 1. Unsubstituted 3,6-bis(2-pyridyl)pyridazine (L) and substituted 3,6-bis(2-pyridl)-4-phenylpyridazine (L^{ph}).

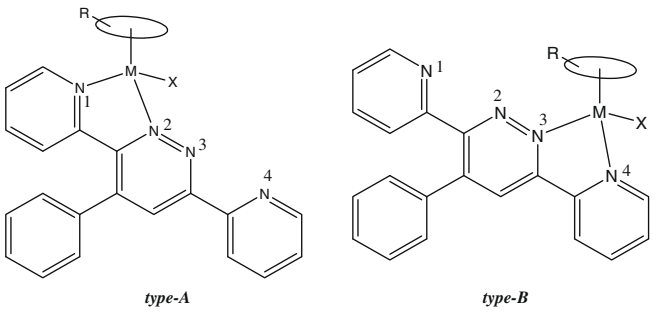

Fig. 2. The two types of complexes [R⟨⟩M(L^{ph})X]$^+$ (M = Ru, Rh and Ir).

(*type-A* + *type-B*) for the same compound is also possible, but not treated in this research.

The reaction of 3,6-bis(2-pyridyl)-4-phenylpyridazine (L^{ph}) with [(η^6-arene)Ru(μ-Cl)Cl]$_2$ (arene = C_6H_6 and *p*-^{i}PrC_6H_4Me), [(η^5-C_5Me_5)Ir(μ-Cl)Cl]$_2$ and [(η^5-Cp)Ru(PPh_3)$_2$Cl] (Cp = C_5H_5, C_5Me_5 and C_9H_7) led to the formation of *type-A* mononuclear complexes. Use of [(η^6-C_6Me_6)Ru(μ-Cl)Cl]$_2$ and [(η^5-C_5Me_5)Rh(μ-Cl)Cl]$_2$ led to the formation of *type-B* complexes. The third possibility (combination of *type-A* and *type-B*) was not borne out in this work. The nature of the bonding modes for the above complexes was elucidated here through NMR and X-ray crystallography. In addition to these studies, we have performed DFT calculations on the complexes **2**, **3**, **4**, **5** and **6** in order to better understand the nature of the bonding modes in the ruthenium, rhodium and iridium complexes with L^{ph}.

To the best of our knowledge, there are yet no reports on half-sandwich platinum group metal complexes with the L^{ph} ligand. The successful formation here of such mononuclear complexes gives promise and scope for the development of *metalla-ligands* or *synthons* based on organometallic systems. Another important factor is the presence of a phenyl ring on the ligand backbone. In the absence of this feature (*viz.*, with the 3,6-bis(2-pyridyl)pyridazine ligand), we were unable to obtain stable and acceptable yields of both mononuclear as well as dinuclear complexes. Due to this, some research groups had suspended further work on such systems, notably those striving to prepare water oxidation catalysts using this ligand [40].

We here report the synthesis of eight new platinum group metal complexes having arenes, Cp* and 3,6-bis(2-pyridyl)-4-phenylpyridazine (L^{ph}) as ligands, all characterized by IR, NMR, mass spectrometry and UV/Visible spectroscopy. The complexes and free ligands were also subjected to density functional theory (DFT) calculations. Molecular structures of three representative complexes (derived from X-ray crystal data) are presented as well.

2. Results and discussion

2.1. Syntheses

The dinuclear arene ruthenium complexes [(η^6-arene)Ru(μ-Cl)Cl]$_2$ (arene = C_6H_6, *p*-^{i}PrC_6H_4Me and C_6Me_6) react with two equivalents of 3,6-bis(2-pyridyl)-4-phenylpyridazine (L^{ph}) in methanol, being stirred at room temperature in the presence of NH_4PF_6 to form the mononuclear arene ruthenium complex cations [(η^6-C_6H_6)Ru(L^{ph})Cl]$^+$ (**1**), [(η^6-*p*-^{i}PrC_6H_4Me)Ru(L^{ph})Cl]$^+$ (**2**), and [(η^6-C_6Me_6)Ru(L^{ph})Cl]$^+$ (**3**) (Scheme 1) and isolated as their hexafluorophosphate salts. The metal atom bonds to the L^{Ph} ligand through the N1 and N2 atoms in the *type-A* complexes **1** and **2**, while in the *type-B* complex **3** the metal bonds through the N3 and N4 atoms of the ligand.

Similarly, reacting the dimeric chloro-bridged complexes [(η^5-C_5Me_5)M(μ-Cl)Cl]$_2$ (M = Rh, Ir) with the same L^{ph} ligand at 50 °C leads to the formation of the mononuclear cationic complexes [(η^5-C_5Me_5)Rh(L^{ph})Cl]$^+$ (**4**) and [(η^5-C_5Me_5)Ir(L^{ph})Cl]$^+$ (**5**) (Scheme 2), isolated as their hexafluorophosphate salts. The metal atom bonds to the L^{Ph} ligand through the N3 and N4 atoms in the *type-B* complex **4**, while in the *type-A* complex **5** the metal bonds *via* the N1 and N2 atoms of the ligand.

The complexes [(η^5-C_5H_5)Ru(PPh_3)$_2$Cl], [(η^5-C_5Me_5)Ru(PPh_3)$_2$Cl] and [(η^5-C_9H_7)Ru(PPh_3)$_2$Cl] reacted with the same L^{ph} ligand in ethanol at 60 °C to form the mononuclear complex cations [(η^5-C_5H_5)Ru(L^{ph})PPh_3]$^+$ (**6**), [(η^5-C_5Me_5)Ru(L^{ph})PPh_3]$^+$ (**7**) and [(η^5-C_9H_7) Ru(L^{ph})PPh_3]$^+$ (**8**) (Scheme 3), isolated as their hexafluorophosphate salts. In all these *type-A* complexes the metal bonds through the N1 and N2 atoms of the ligand.

Complexes **1**, **2** and **3** are orange-yellow, **4** and **5** are dark yellow, while **6**, **7** and **8** are orange-brown in color. All are non-hygroscopic, air-stable solids soluble in acetonitrile and partially soluble in dichloromethane, chloroform, methanol and acetone. All complexes have been characterized on the basis of elemental analysis, ^{1}H NMR, IR, UV–Visible spectroscopy and mass spectrometry.

The infrared spectra of complexes **1–8** exhibit a strong band in the region 844–850 cm^{-1}, a typical ν_{P-F} stretching band for the PF_6 anions. Besides this, peaks were observed which correspond to the phenyl, pyridyl and pyridazine rings (C=C and C=N moieties). The mass spectra display peaks with *m/z* at 580, 525, 573, 554, 638, 743, 818 and 789, corresponding to the molecular ion M^+ peaks for complexes **1**–**8**, respectively.

2.2. NMR studies

The ^{1}H NMR spectrum of the free (unbound) ligand L^{ph} exhibits resonances at δ 8.80 (d, 6-H), 8.74 (d, 6′-H), 8.67 (s, 9-H), 8.49 (d, 3-H) 7.94 (td, 3′,4-H), 7.80 (td, 4′-H), 7.44 (m, Ph-H), 7.34 (dd, 5-H), 7.28 (dd, 5′-H) in $CDCl_3$. Upon coordination with metal atoms, the ^{1}H NMR spectrum of the L^{ph} ligand protons exhibits two different sets of resonances for the two different types of complexes. The *type-A* complexes **1**, **2**, **5**, **6**, **7** and **8** show one type of spectral resonance (see Fig. 3), while the *type-B* complexes **3** and **4** show a different set of resonances (see Fig. 4) for the aromatic regions of the ligand.

Type-A: The ^{1}H NMR spectra of the Ru(II)L^{ph} and Ir(III)L^{ph} complexes **1**, **2** and **5–8** exhibit ten sets of resonances at ~δ 9.54 (d, 6-H), 8.76 (d, 6′-H), 8.72 (d, 3-H), 8.21 (s, 9-H), 8.18 (td, 4-H), 7.57 (td, 4′-H), 7.37 (td, 5-H), 7.30 (m, ph-H), 7.15 (td, 5′-H) and 6.79 (d, 3′-H) ppm for the protons of the L^{ph} ligand in CD_3CN-d_3. The resonances of the protons 6, 6′, 3 and 4 of ligand L^{ph} are shifted downfield by $\delta \sim 0.75$, 0.10, 0.32 and 0.31, respectively with respect to the free ligand. As an example, the NMR spectrum of the *type-A* complex **6** is presented in Fig. 3.

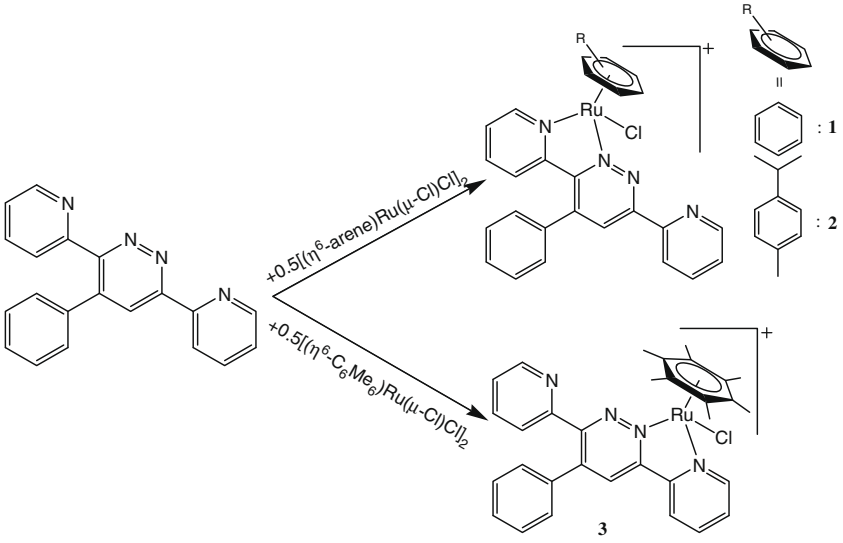

Scheme 1.

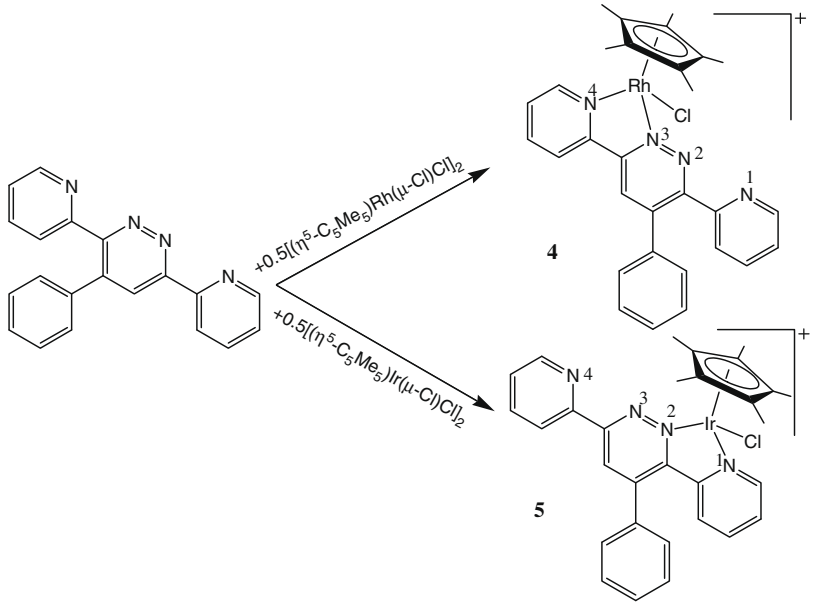

Scheme 2.

Type-B: The ^{1}H NMR spectra of the Ru(II) and Rh(III) complexes $[(\eta^6\text{-}C_6Me_6)Ru(L^{ph})Cl]^+$ (**3**) and $[(\eta^5\text{-}C_5Me_5)Rh(L^{ph})Cl]^+$ (**4**) exhibit eight sets of resonances at δ = 8.91 (d, 6′-H), 8.82 (d, 6-H), 8.67 (s, 9-H), 8.59 (d, 3′-H), 8.04 (td, 4′-H), 7.67-7.61 (m, 5 and ph-H), 7.53 (td, 4 and 5′-H) and δ = 8.91 (d, 6′-H), 8.59 (d, 6-H), 8.41 (s, 9-H), 8.39 (d, 3′-H), 8.19 (td, 4′-H), 7.81 (m, 4 and 5′-H), 7.68 (d, 3-H), 7.66–7.61 (m, 5 and ph-H) ppm in $CDCl_3$ (Fig. 4a and b). The resonances of protons 6′, 9, 3′ and 4′ of the ligand are shifted downfield by $\delta \approx 0.17$, 0.01, 0.55 and 0.21 ppm, respectively (with respect to the corresponding free L^{ph} protons) due to the inductive effect of the metal [20]. The significant downfield shift of proton 9 of ligand L^{ph} reveals the formation of *type-B* complexes as compared to the previous type.

We choose to distinguish the two types of complex on the basis of NMR, and present the spectra of the *type-B* complexes **3** and **4** (Fig. 4a and b). This furnishes the evidence for the formation of complex **3** with the *type-B* bonding mode in ruthenium complexes having the hexamethylbenzene co-ligand. This is not the case with ruthenium complexes having the η^6-*p*-^{i}PrC$_6$H$_4$Me and η^6-C$_6$H$_6$ co-ligands, where Ru–L^{Ph} bonding occurs in *type-A* fashion. Similar results for other complexes (based on reactivity studies) were observed earlier in our research group, where complexes containing the hexamethylbenzene co-ligand contrast clearly with those containing the η^6-*p*-^{i}PrC$_6$H$_4$Me and η^6-C$_6$H$_6$ ligands [41,42].

Furthermore, the aromatic regions of L^{ph} ligand signals complex **2** exhibit a singlet at δ = 2.28 for the methyl protons, a septet at δ = 2.82 for the CH proton of the isopropyl group, two doublets for the diastereotopic methyl protons of the isopropyl group, and likewise four doublets for the diastereotopic CH protons of the *p*-cymene ligand. Complexes **1** and **3** exhibit a singlet for the protons of the benzene ring and protons of the hexamethylbenzene at δ 6.18 and 2.18, respectively. Complexes **4** and **5** exhibit a singlet for the methyl protons of the pentamethylcyclopentadienyl ligand at δ 1.77 and 1.68, respectively. Complexes **6** and **7** exhibit a singlet at δ 4.91 and 2.03 for the protons of the cyclopentadienyl ligand and the methyl protons of pentamethylcyclopentadienyl ligand,

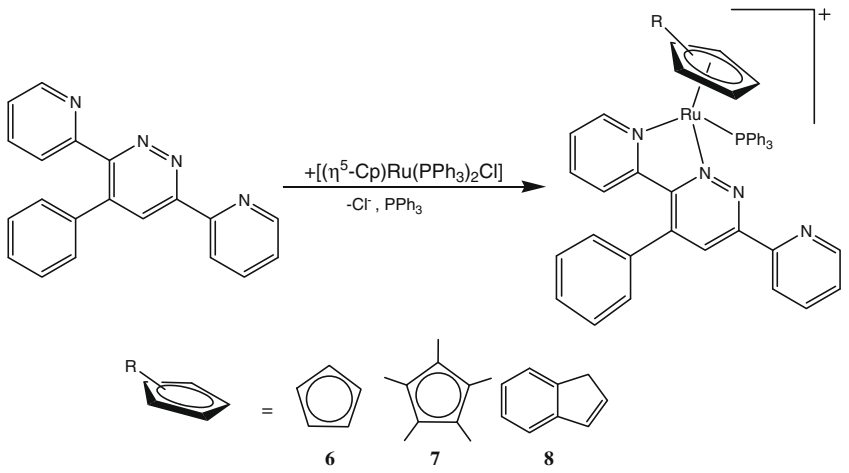

Scheme 3.

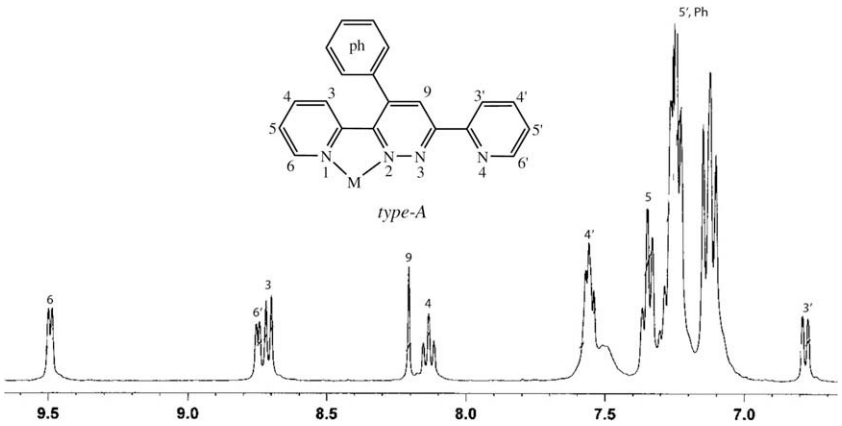

Fig. 3. Aromatic region of the ^{1}H NMR spectrum of complex **6** (*type-A*) in $CDCl_3$.

respectively. Complex **8** exhibits three characteristic sets of signals (multiplet, triplet and doublet) for the protons of the indenyl ligand. The protons of the triphenylphosphine ligand exhibit a multiplet at δ 7.22–7.55. The ^{31}P{1H} NMR spectra of complexes **6**, **7**, and **8** show chemical shifts at δ 46.12, 49.21, and 48.42, respectively, which indicate that each metal atom is bonded with a single triphenylphosphine ligand.

2.3. Molecular structures

The molecular structures of $[(\eta^6\text{-}p\text{-}^i PrC_6H_4Me)Ru(L^{ph})Cl]^+$ (**2**), $[(\eta^5\text{-}C_5Me_5)Rh(L^{ph})Cl]^+$ (**4**) and $[(\eta^5\text{-}C_5H_5)Ru(L^{ph})(PPh_3)]^+$ (**6**) have been established by single-crystal X-ray analysis of their hexafluorophosphate salts (Tables 1 and 2). The complexes show a typical piano-stool geometry with the metal center coordinated to the arene ligand, to the chelating L^{ph} ligand, and to a terminal chloride in complexes **2** and **4**, and triphenylphosphine in complex **6**. The metal atom is in an octahedral arrangement with the two *cis*-nitrogen atoms of the L^{ph} ligand acting as a bidentate chelating ligand through the two neighboring pyridyl and pyridazinyl nitrogen atoms. In principle, in mononuclear complexes, tetradentate ligands such as L or L^{ph} can coordinate to the metal center either through the N1 and N2 atoms (*type-A*) or the N3 and N4 atoms (*type-B*). It is fascinating to observe here that the crystal structures of complexes **2** and **6** are found to be N1,N2-coordinated (*type-A*), while the complex **4** is found to be N3,N4-coordinated (*type-B*) in a five-membered ring chelating fashion involving the nitrogen atom of the pyridine moiety and one nitrogen atom of the pyridazinyl moiety. This could be due to the steric interactions of arene ligands, electronic factors, the nature of the co-ligands, the oxidation state of the metal atom and the symmetry of the ligand. The nature of these bonding modes is studied here by density functional theory (see later). The molecular structures of complexes **2**, **4** and **6** are shown in Figs. 5–7, respectively, with the bond lengths and angles presented in Table 1.

In the mononuclear complexes **2, 4** and **6** the nitrogen-metal distances (2.073, 2.120 and 2.086 Å) associated with the pyridyl ligand are slightly longer than the corresponding pyridazinyl ligand nitrogen-metal distance (2.045, 2.084 and 2.076 Å). These are comparable to those in the previously studied complexes $[(\eta^6\text{-}p\text{-}^i PrC_6H_4Me)RuCl(2,3\text{-bis}(2\text{-pyridyl})\ \text{pyrazine})]BF_4$ [43], $[Rh_2(L\text{-}H)(NBD)(\eta^1\text{-}C_7H_7)(CH_3OH)(CH_3CN)](BF_4)_2$ [44], and $[(\eta^6\text{-}p\text{-}^i PrC_6H_4Me)Ru(2\text{-}(2\text{-pyridyl})\text{-}1,8\text{-naphthyridine})Cl]PF_6$ [45]. The Rh–N distances (2.120(3) and 2.084(3) Å) in **4** are slightly longer than the corresponding distances in complex **2** (2.073(3) and 2.045(2) Å) and complex **6** (2.076 and 2.086). The M–Cl bond lengths [2.387(10) and 2.384(13)] show no significant differences between values for the cations studied here and other reported values [46]. The N–M–N bond angles [76.1(11)° in **2** and 76.0(13)° in **4** are similar in value to that [76.2(2)°] observed in the complex $[(\eta^6 p\text{-}^i PrC_6H_4Me)RuCl(2,3\text{-bis}(\alpha\text{-pyridyl})quinoxaline)]^+$ [47].

In complex **2**, the distance between the ruthenium atom and the centroid of the $\eta^6\text{-}p\text{-}^i PrC_6H_4Me$ ring is 1.693 Å. In complex **4**, the distance between the rhodium atom and the centroid of the

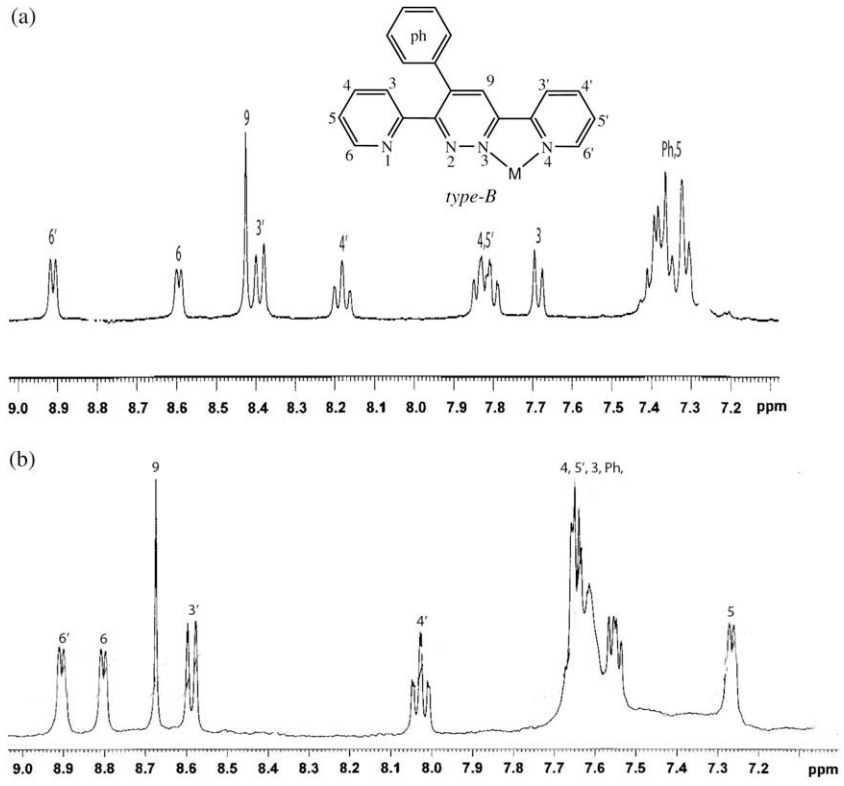

Fig. 4. Aromatic regions of the ^{1}H NMR spectra of (a) complex **4**; (b) complex **3** (*type-B*) in $CDCl_3$.

Table 1
Selected bond lengths (Å) and bond angles (°) for complexes **2**, **6** and **4**.

	Complex **2**	Complex **6**	Complex **4**	
Bond distances				
Ru–N1	2.073(3)	2.086(3)	Rh–N4	2.120(3)
Ru–N2	2.045(3)	2.076(3)	Rh–N3	2.084(3)
Ru–Cl1	2.387(10)	2.308(10)	Rh–Cl1	2.384(13)
Ru–centroid (arene)	1.693	1.843	Rh–centroid (Cp* ring)	1.789
C9–C10	1.483(5)	1.466(5)	C9–C10	1.471(5)
C5–C6	1.479(5)	1.490(6)	C5–C6	1.500(5)
N2–N3	1.334(4)	1.340(4)	N3–N4	1.330(4)
Bond angles				
N1–Ru–N2	76.11(11)	76.11(2)	N2–Rh–N3	76.00(13)
N1–Ru–Cl1	83.91(9)	95.75(9)	N4–Rh–Cl1	83.50(10)
N2–Ru–Cl1	84.95(8)	89.97(9)	N3–Rh–Cl1	88.73(10)
Ru1–N2–C9	119.83	118.9(3)	Rh1–N3–C9	117.99
Ru1–N2–N3	117.16	117.9(2)	Rh1–N3–N2	120.35
Ru1–N1–C10	117.61	116.7(2)	Rh1–N4–C10	116.03

η^5-C_5Me_5 ring is 1.789 Å, while the distance between the ruthenium atom and the η^5-C_5H_5 ring is 1.843 Å. These bond distances are comparable to those in the related complex cations [(η^6-*p*-^{i}PrC$_6$H$_4$Me)Ru(pyNp)Cl]PF$_6$, [(η^5-C_5Me_5)Ir(pyNp)Cl]PF$_6$ (PyNp = 2-(2-pyridyl)-1,8-naphthyridine) (1.68 and 1.79 Å) [45], [(η5-C_5Me_5)RhCl(C_5H_4N–2CH=N–C_6H_4-*p*-Cl)]$^+$ [48] and [Ru(η^5-C_5H_5)(PPh_3)(κ^2-paa)]$^+$ and [Ru(η^5-C_5H_5)(κ^1-dppm)(κ^2-paa)]$^+$ [49]. The solid state molecular structures of representative complexes **2**, **4** and **6** are presented in Figs. 5–7, respectively.

2.4. Theoretical calculations

All calculations on the molecular species studied were carried out using the B3LYP DFT method and different basis sets. All species were subjected to full geometry optimization.

Table 2
Crystallographic and structure refinement parameters for complexes **2**, **4** and **6**.

Complex	**2**·$CHCl_3$	**4**	**6**
Chemical formula	$C_{31}H_{29}Cl_4N_4RuPF_6$	$C_{30}H_{29}ClN_4RhPF_6$	$C_{43}H_{34}F_6N_4P_2Ru$
Crystal system	Triclinic	Monoclinic	Monoclinic
Space group	$P\bar{1}$ (no. 2)	$P2_1/n$ (no. 14)	$P2(1)/c$
Crystal color and shape	Orange block	Red block	Red block
Crystal size (mm^3)	0.23 × 0.17 × 0.16	0.28 × 0.23 × 0.18	0.50 × 0.26 × 0.15
a (Å)	10.4283(19)	9.244(3)	10.1059(2)
b (Å)	11.247(2)	14.147(5)	20.6495(4)
c (Å)	15.491(3)	23.425(8)	18.8735(4)
α (°)	85.104(3)		
β (°)	81.287(3)	95.900(6)	94.3950(10)
γ (°)	71.700(3)		
V (Å^3)	1703.8(5)	3047.4(18)	3926.97(14)
Z	2	4	4
T (K)	173(2)	173(2)	293(2) K
D_x (g/cm^3)	1.648	1.589	1.495
μ (mm^{-1})	0.883	0.765	0.546
Scan range (°)	2.28 < θ < 25.95	2.26 < θ < 25.60	1.46 < θ < 28.29
Unique reflections	6597	5963	9046
Reflections used [$I > 2\sigma(I)$]	5719	4684	5505
R_{int}	0.0260	0.0426	0.0376
Final R indices [$I > 2\sigma(I)$]*	0.0452, wR_2 = 0.1264	0.0496, wR_2 = 0.1267	0.0568, wR_2 = 0.1560
R indices (all data)	0.0518, wR_2 = 0.1323	0.0642, wR_2 = 0.1355	0.1004, wR_2 = 0.1778
Goodness-of-fit (GOF)	1.005	1.068	1.048
Max, min $\Delta\rho$ (e Å^{-3})	0.864, −0.710	0.807, −0.543	0.953, −0.797

* Structures were refined on F_o^2: $wR_2 = [\sum[w(F_o^2 - F_c^2)^2]/\sum w(F_o^2)^2]^{1/2}$, where $w^{-1} = [\sum(F_o^2) + (aP)^2 + bP]$ and $P = [\max(F_o^2, 0) + 2F_c^2]/3$.

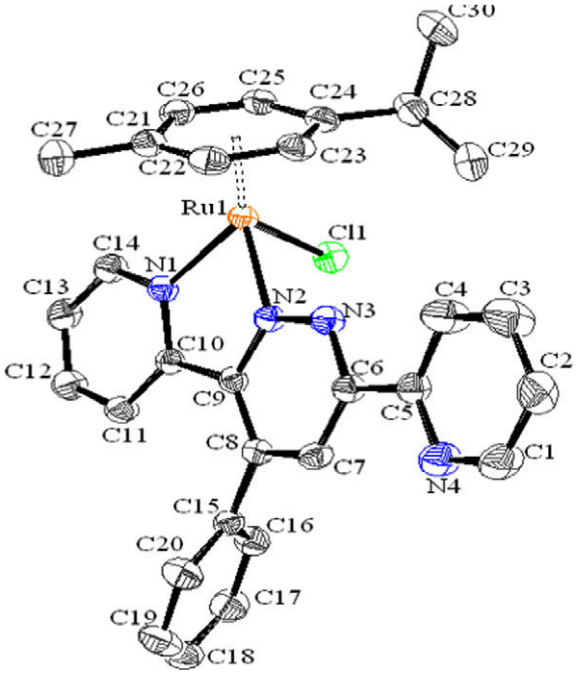

Fig. 5. Molecular structure of a complex **2** at 35% probability level. Hydrogen atoms, chloroform molecule and hexafluorophosphate anion have been omitted for clarity.

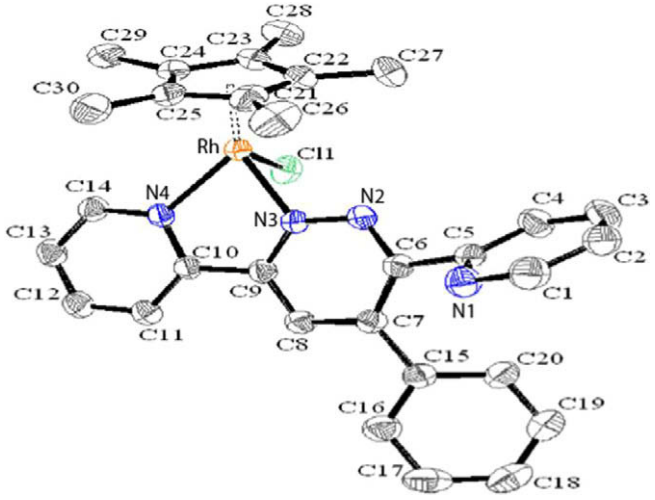

Fig. 6. Molecular structure of complex **4** at 35% probability level. Hydrogen atoms and hexafluorophosphate anion have been omitted for clarity.

2.4.1. L and L^{ph} ligand structures

We have performed DFT calculations using the B3LYP/6-31+G** strategy to determine the effect of the phenyl substituent on the nitrogen atoms of the central pyridazine and pyridine rings. Firstly, both the ligands L and L^{ph} in their free state were optimized in the low-energy *anti* orientation [Fig. SF1a and c (Supplementary material)]. Since these ligands occur in the *syn* conformer in complexes **2**, **4** and **6**, they were also optimized in the higher energy *syn* orientation (Fig. SF1b and d). The *anti* conformer of L is planar but the *syn* conformer is non-planar with the N–C–C–N dihedral being 83.8° [Table S1 (Supplementary material)]. On the other hand, both *anti* and *syn* orientations of L^{ph} are non-planar, due to the effect of the phenyl substituent on the central pyridazine ring. The dihedral angles N1–C2–C3–N2 and N3–C6–C7–N4 are, respectively, found to be 141.3° and 179.2° for *anti* L^{Ph}, and −62.9° and −47.2° for

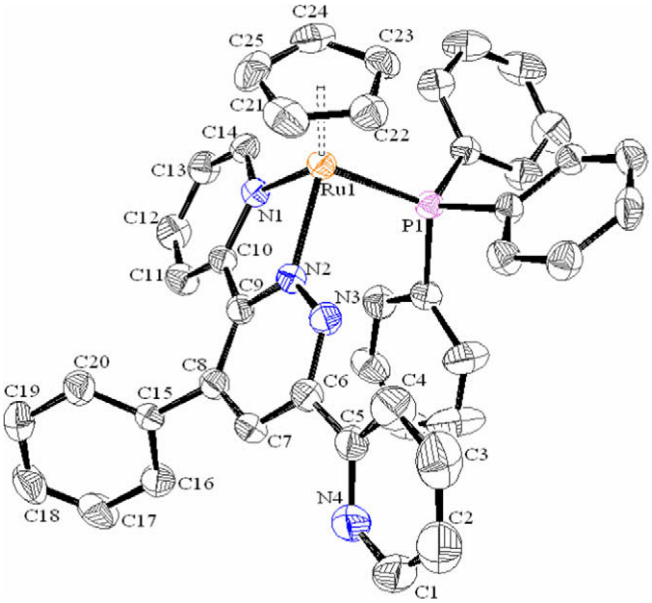

Fig. 7. Molecular structure of complex **6** at 35% probability level. Hydrogen atoms and hexafluorophosphate anion have been omitted for clarity.

syn L^{Ph} (Table S1). These values are very close to the experimental values [34]. In terms of energy, *anti* L is 14.33 kcal/mol more stable than *syn* L while *anti* L^{ph} is 9.68 kcal/mol [Table S2 (Supplementary material)] more stable than *syn* L^{ph}. The coordinated L^{ph} ligand in complexes **2** and **4** is in the *syn* conformation.

The electronic charges on the nitrogen atoms in the *anti* L^{ph} conformation reveal that atoms N3 and N4 have more negative charge than atoms N1 and N2 (see Fig. SF1c). This suggests that presence of the phenyl group affects the electronic charges on the four nitrogen atoms as well as the dihedral angles of the pyridine and pyridazine rings, so that the N3–N4 (*type-B*) binding site is more electron-rich than the N1–N2 (*type-A*) bonding site.

2.4.2. Structures of complexes

In order to gain further insight into the bonding modes in the ruthenium, rhodium and iridium complexes, we have carried out a detailed investigation using density functional theory. The key findings are described in the following sections.

B3LYP/LanL2DZ calculations with full geometry optimization were undertaken for the cationic species **2**, **4** and **6** in both *type-A* and *type-B* bonding modes as depicted in Fig. SF2 of the supporting information, where the crystal structure geometries provided the starting input for optimization. The other species **3** and **5** were subjected to calculation using appropriate modifications of the geometries of **2**, **4** and **6**. The calculated geometrical parameters of the above complexes [Table S3 (Supplementary material)] are found to be in close agreement with the experimental values obtained from X-ray crystallographic study (Table 1). From Table S3 of Supplementary material we can see that the positions of binding have discernible effects on the stability and geometrical structure of the complexes. Comparing the computed results of the parent complexes **2**, **3**, **4**, **5**, **6** with the experimental data (see Table 1), we find that the computed coordination bond lengths (Ru–N) are shorter than the corresponding experimental value by 1–3%, the largest differences being found for the metal–arene carbon distances [50]. Computed coordinated bond angles are wider by 2% than those found experimentally. At the same time, the computed mean bond lengths C–C(N) of the ligand skeletons of these complexes are close to the general bond lengths. We thereby deduce

that the structures obtained from these DFT calculations are reliable.

The 3,6-bis(2-pyridyl)-4-phenylpyridazine (L^{ph}) ligand has two bidentate binding sites, *viz*., the N1 and N2 atoms (*type-A*) and the N3 and N4 atoms (*type-B*). In principle, the metal atom should prefer the *type-A* mode (atoms N1 and N2), since the substituents of the pyridazine ring (phenyl and pyridine rings) are *meta* with respect to N2, and the dihedral angle N1–C2–C3–N2 for the *anti* conformer of L^{ph} (141.3°) is found to be less than the dihedral angle N3–C6–C7–N4 (179.2°). On the other hand, for the *type-B* bonding mode (at atoms N3 and N4), the substituents of the central pyridazine ring (phenyl and pyridine rings) are, respectively, *para* and *meta* with respect to N3. The dihedral angle N3–C6–C7–N4 (179.2°) is found to be noticeably greater than the dihedral angle N1–C2–C3–N2 (141.3°) (see Table S3). These results suggest that the metal atom prefers to bind through the N1 and N2 atoms (*type-A*) rather than through the N3 and N4 atoms (*type-B*).

On the other hand, the Mulliken atomic charges on the N3 and N4 atoms of ligand L^{ph} are more negative than for the N1 and N2 atoms (see Fig. SF1c). This means that atoms N3 and N4 should be better electron donors towards the metal center than atoms N1 and N2, implying that formation of *type-B* complexes is more favorable than *type-A* complexes. Interestingly, experimental results reveal that complexes **3** and **4** favor the *type-B* bonding mode while all the other complexes favor the *type-A* mode. Possible reasons could be the size of the metal atom, oxidation state of the complex, symmetry of the ligand and nature of the substituents on the metal atom.

The molecular structure of complex $[(\eta^6\text{-}p\text{-}^i PrC_6H_4Me)Ru(L^{ph})Cl]^+$ **2** shows κ^2 type coordination in the *type-A* bonding mode (see Fig. 6). This geometry was optimized for both *type-A* and *type-B* bonding modes. The results reveal that the *type-A* bonding mode is 1.25 kcal/mol more stable than *type-B*. Replacing $p\text{-}^i PrC_6H_4Me$ of **2** with the more electron-rich hexamethylbenzene (C_6Me_6) ligand gives the complex **3** $[(\eta^6\text{-}C_6Me_6)Ru(L^{ph})Cl]^+$. The geometry of this complex was built up by modification of complex **2** in both conformations, being optimized at the B3LYP level with a LanL2DZ basis set (Fig. SF2 3A and B). The results reveal that the *type-B* structure is 0.96 kcal/mol more stable than the *type-A* structure. These trends suggest that the nature of the co-ligands impacts on the bonding mode of the L^{ph} ligand. Since the energy difference between *type-A* and *type-B* [see Table S4 (Supplementary material)] structures is quite low, packing and other environmental factors may affect preference of one form over the other. The molecular structure of $[(\eta^5\text{-}C_5Me_5)Rh(L^{ph})Cl]PF_6$ **4** shows a κ^2 type of coordination with the *type-B* bonding mode (see Fig. 6). The geometry was optimized for both *type-A* and *type-B* bonding modes (*Fig.* SF2 4A and B), where the results predict the *type-A* structure as 0.95 kcal/mol less stable than the *type-B* structure. Replacing rhodium in $[(\eta^5\text{-}C_5Me_5)Rh(L^{ph})Cl]PF_6$ **4** with the larger atom iridium gives $[(\eta^5\text{-}C_5Me_5)Ir(L^{ph})Cl]PF_6$ **5**, where the energy of the *type-A* structure is 0.35 kcal/mol lower in energy than the *type-B* structure (*Fig.* SF2 5A and B). This suggests that size of the metal atom also has a significant effect on the preferred choice of bonding mode.

In order to study the effect of steric interactions on the choice of bonding mode, we replaced the $p\text{-}^i PrC_6H_4Me$ and chloride ligands in complex **2** with the less electron-rich (but sterically free) cyclopentadienyl ligand and the bulky triphenylphosphine ligand, respectively, giving the complex **6**. Calculated energies of the optimized geometries (*Fig.* SF2 6A and B) reveal that the *type-A* structure of **6** is 1.96 kcal/mol more stable than the *type-B* structure. This suggests that steric factors do not have much impact on the choice of bonding mode (see *Table* S4).

In conclusion, the calculated energies of the optimized geometries of complexes **2**, **3**, **4**, **5** and **6** reveal that the preferred choice of binding mode neither depends on the steric nature of the co-ligands nor on the oxidation state of the complex. However, the optimized geometries of **4** and **5** reveal that size of the metal atom does have a significant impact on choice of binding mode, where the rhodium complex **4** favors the *type-B* bonding mode while the iridium complex **5** favors the *type-A* bonding mode (substituents or co-ligands and oxidation state being the same). In addition to the effect of the size of the metal atom, the nature of the co-ligand also has an impact on the choice of bonding mode because complexes with less electron-rich donor co-ligands favor the *type-A* bonding mode (**1** and **2** and **5**–**8**) while complexes having more electron-rich donor co-ligands favor the *type-B* bonding mode (**3** and **4**). These DFT results thus elucidate the effects of the size of the metal atom, the nature of the co-ligands and various electronic factors on the nature of bonding mode.

2.5. UV/Visible spectroscopy

Electronic absorption spectral data of complexes **1**–**8** at 10^{-5} M concentration in the range 290–600 nm are summarized in Table 3. The spectra of these complexes are characterized by two main features, *viz*., an intense ligand-localized or intra-ligand $\pi \rightarrow \pi^*$ transition in the ultraviolet region, and metal-to-ligand charge transfer (MLCT) $d\pi(M) \rightarrow \pi^*$ (L^{ph} ligand) bands in the visible region [51]. Since the low spin d^6 configuration of the mononuclear complexes provides filled orbitals of proper symmetry at the Ru(II), Rh(III) and Ir(III) centers, these can interact with low lying π^* orbitals of the ligands. All these complexes show an intense band in the region 290–320 nm and a low-energy absorption band in the visible region 420–445 nm. In addition to these two absorption bands, an additional low intensity band at 350 nm and a shoulder type band

Table 3
UV/Visible spectral data for selected complexes in acetonitrile at 298 K.

Complex no.	Complex	λ_{max} (nm)/ε 10^{-5} M^{-1} cm^{-1}
1	$[(\eta^6\text{-}C_6H_6)Ru(L^{ph})Cl]^+$	306 (0.47) 412
2	$[(\eta^6\text{-}p\text{-}^i PrC_6H_4Me)Ru(L^{ph})Cl]^+$	320 (0.65) 420
3	$[(\eta^6\text{-}C_6Me_6)Ru(L^{ph})Cl]^+$	317 (0.61) 412
4	$[(\eta^5\text{-}C_5Me_5)Rh(L^{ph})Cl]^+$	299 (0.49) 349 (0.15) 420
5	$[(\eta^5\text{-}C_5Me_5)Ir(L^{ph})Cl]^+$	300 (0.51) 380 470
6	$[(\eta^5\text{-}C_5H_5)Ru(L^{ph})PPh_3]^+$	290 (0.61) 435(0.15)
7	$[(\eta^5\text{-}C_9H_7)Ru(L^{ph})PPh_3]^+$	294 (0.36) 445

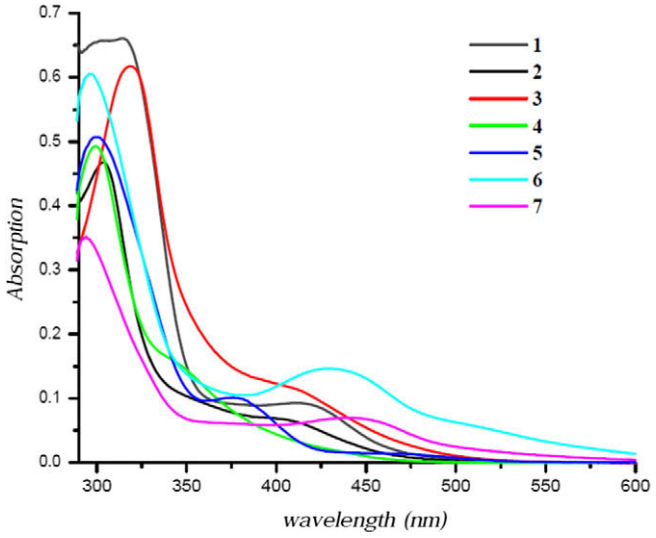

Fig. 8. UV/Visible electronic spectra of complexes in acetonitrile at 298 K.

at 280 nm for complexes **4** and **5**, respectively are observed. The high intensity band in the UV region is assigned to inter- and intra-ligand π–π^* transitions [52,53], while the low-energy absorption band in the visible region is assigned to metal-to-ligand charge transfer (MLCT) (t_{2g}–π^*). Spectra of these complexes are presented in Fig. 8.

3. Experimental

All solvents were dried and distilled prior to use. 2-Cyanopyridine and phenyl acetylene (Aldrich) were purchased and used as received. The complexes $[(\eta^6\text{-}C_6H_6)Ru(\mu\text{-}Cl)Cl]_2$, $[(\eta^6\text{-}p\text{-}^iPrC_6H_4Me)Ru(\mu\text{-}Cl)Cl]_2$, $[(\eta^6\text{-}C_6Me_6)Ru(\mu\text{-}Cl)Cl]_2$ [54–56], $[(\eta^5\text{-}C_5Me_5)M(\mu\text{-}Cl)Cl]_2$ (M = Rh, Ir) [57–59], $[(\eta^5\text{-}C_5H_5)Ru(PPh_3)_2Cl]$ and $[(\eta^5\text{-}C_9H_7)Ru(PPh_3)_2Cl]$ [60,61] were prepared according to literature methods. The ligand L^{ph} was prepared by the Diels–Alder reaction of 3,6-bis(2-pyridyl)tetrazine with phenyl acetylene [62]. NMR spectra were recorded on an AMX-400 MHz spectrometer. Infrared spectra were recorded as KBr pellets on a Perkin–Elmer 983 spectrophotometer, while elemental analyses of the complexes were performed on a Perkin–Elmer-2400 CHN/S analyzer. Mass spectra were obtained from Waters ZQ 4000 mass spectrometer by the ESI method. Absorption spectra were obtained at room temperature using a Perkin–Elmer Lambda 25 UV/Visible spectrophotometer.

3.1. General procedure for preparation of mononuclear complexes **1**–**3**

A mixture of $[(\eta^6\text{-arene})Ru(\mu\text{-}Cl)Cl]_2$ (arene = C_6H_6, $p\text{-}^iPrC_6H_4Me$ and C_6Me_6) (0.07 mmol), ligand L^{ph} (0.15 mmol) and 2.5 equivalents of NH_4PF_6 in dry methanol (15 ml) was stirred at room temperature for 6 h. The precipitate was separated by filtration, washed with cold methanol, diethyl ether and dried under vacuum.

3.1.1. $[(\eta^6\text{-}C_6H_6)Ru(L^{ph})Cl]PF_6$ (**1**)

Orange-yellow solid, yield 80 mg (89%): Anal. Calc. for $C_{26}H_{20}ClN_4RuPF_6$ (669.5): C, 46.61; H, 3.01; N, 8.36. Found: C, 46.68; H, 3.18; N, 8.48%. ^{1}H NMR (400 MHz, CD_3CN, 25 °C): δ = 9.57 (d, 1H, J_{H-H} = 5.58 Hz), 8.86 (d, 1H, J_{H-H} = 8 Hz), 8.31 (s, 1H), 8.26 (d, 1H), 8.18 (td, 1H), 8.08 (td, 2H), 7.71 (td, 1H), 7.53–7.51 (m, 5H), 7.25 (d, 1H), 6.18 (s, 6H, C_6H_6) ppm. ESI-MS (*m*/*z*): 525.1 (100%) $[M-PF_6]^+$, 489.1 (10%) $[M-PF_6\_Cl]^+$. IR (KBr, cm^{-1}): $\nu_{(P-F)}$ 844s; 558m.

3.1.2. $[(\eta^6\text{-}p\text{-}^iPrC_6H_4Me)Ru(L^{ph})Cl]PF_6$ (**2**)

Dark orange solid, yield 80 mg (89%): Anal. Calc. for $C_{30}H_{28}ClN_4RuPF_6$ (726.05): C, 49.63; H, 3.89; N, 7.72. Found: C, 50.08; H, 3.78; N, 7.95%. ^{1}H NMR (400 MHz, CD_3CN, 25 °C): δ = 9.42 (d, 1H, J_{H-H} = 5.60 Hz), 8.78 (dd, 2H, J_{H-H} = 8 Hz), 8.28 (s, 1H), 8.15(dt, 1H), 7.75 (td, 1H), 7.58–7.63 (m, 5H),7.43 (td, 2H), 7.20 (d, 1H, J_{H-H} = 8 Hz), 6.04 (d, 1H), 6.01 (d, 1H), 5.85 (d, 1H), 5.81 (d, 1H), 2.82 (sept, 1H, $CH(CH_3)_2$), 2.28 (s, 3H, CH_3), 1.18 (d, 3H, $CH(CH_3)_2$), 1.14 (d, 3H, $CH(CH_3)_2$) ppm. ESI-MS (*m*/*z*): 580.8 (100%) $[M-PF_6]^+$, 544.7 (20%) $[M-PF_6\_Cl]^+$. IR (KBr, cm^{-1}): $\nu_{(P-F)}$ 842s; 558m.

3.1.3. $[(\eta^6\text{-}C_6Me_6)Ru(L^{ph})Cl]PF_6$ (**3**)

Orange-yellow solid, yield 80 mg (89%): Anal. Calc. for $C_{32}H_{32}ClN_4RuPF_6$ (754.1): C, 50.97; H, 4.28; N, 7.43. Found: C, 51.08; H, 4.31; N, 7.29%. ^{1}H NMR (400 MHz, CD_3CN, 25 °C): δ = 8.91 (d, 1H, J_{H-H} = 5.58 Hz), 8.82 (d, 1H, J_{H-H} = 8 Hz), 8.67 (s, 1H), 8.59 (d, 1H, J_{H-H} = 8 Hz), 8.04 (td, 1H), 7.67–7.61 (m, 7H), 7.53 (td, 2H), 2.18 (s, 18H, $C_6(Me)_6$) ppm. ESI-MS (*m*/*z*): 608.9 (100%) $[M-PF_6]^+$, 573.6 (30%) $[M-PF_6\_Cl]^+$. IR (KBr, cm^{-1}): $\nu_{(P-F)}$ 845; 558m.

3.2. General procedure for preparation of mononuclear complexes **4** and **5**

A mixture of $[(\eta^5\text{-}C_5Me_5)M(\mu\text{-}Cl)Cl]_2$ (M = Rh, Ir) (0.07 mmol), ligand L^{ph} (0.18 mmol) and 2.5 equivalents of NH_4PF_6 in dry methanol (15 ml) was refluxed for 4 h. The reaction mixture was cooled over-night at room temperature, during which time the crystalline compound was formed. It was separated by filtration, washed with cold methanol, diethyl ether and dried under vacuum.

3.2.1. $[(\eta^5\text{-}C_5Me_5)Rh(L^{ph})Cl]PF_6$ (**4**)

Dark yellow color, yield 80 mg (77%): Anal. Calc. for $C_{30}H_{29}ClN_4RhPF_6$ (728.9): C, 49.43; H, 4.01; N, 7.69. Found: C, 50.10; H, 3.99; N, 7.65%. ^{1}H NMR (400 MHz, $CDCl_3$, 25 °C): δ = 8.91 (d, 1H, J_{H-H} = 8 Hz), 8.59 (d, 1H), 8.41 (s, 1H), 8.39 (d, 1H), 8.19 (td,1H), 7.81 (m, 2H), 7.68 (d, 1H), 7.66–7.61 (m, 5H), 7.40 (d, 1H), 1.77 (s, 15H, C_5Me_5) ppm. ESI-MS (*m*/*z*): 583.1 (100%) $[M-PF_6]^+$, 558.1 (23%) $[M-PF_6\_Cl]^+$. IR (KBr, cm^{-1}): $\nu_{(P-F)}$ 845s; 558m.

3.2.2. $[(\eta^5\text{-}C_5Me_5)Ir(L^{ph})Cl]PF_6$ (**5**)

Dark yellow color, yield 70 mg (83%): Anal. Calc. for $C_{30}H_{29}ClN_4IrPF_6$ (818.2): C, 44.04; H, 3.57; N, 6.85. Found: C, 44.10; H, 3.59; N, 6.79%. ^{1}H NMR (400 MHz, $CDCl_3$, 25 °C): δ = 9.30 (d, 1H, J_{H-H} = 8 Hz), 8.88 (dd, 2H, J_{H-H} = 6.8 Hz), 8.71 (s, 1H), 8.45 (td, 1H), 8.22 (td, 2H), 7.84 (td, 1H), 7.75 to 7.67 (m, 5H), 7.53 (d, 1H), 1.68 (s, 15H, C_5Me_5) ppm. ESI-MS (*m*/*z*): 673.3 (100%) $[M-PF_6]^+$, 638.1 (32%) $[M-PF_6\_Cl]^+$. IR (KBr, cm^{-1}): $\nu_{(P-F)}$ 845s; 558m.

3.3. General procedure for preparation of mononuclear complexes **6**–**8**

A mixture of $[(Cp)Ru(PPh_3)_2Cl]$ (Cp = C_5H_5, C_5Me_5, C_9H_7) (0.07 mmol), ligand L^{ph} (0.08 mmol) and 1.5 equivalents of NH_4PF_6 in dry ethanol (15 ml) was refluxed for 14 h. The color changed from a dark yellow to a dark red color. The reaction mixture was cooled over-night at room temperature during which time the crystalline compound was formed. Some of the crystals were found suitable for X-ray crystal study. The product was separated by filtration, washed with cold ethanol, diethyl ether and dried under vacuum.

3.3.1. $[(\eta^5\text{-}C_5H_5)Ru(L^{ph})(PPh_3)]PF_6$ (**6**)

Orange color, yield 60 mg (63%): Anal. Calc. for $C_{43}H_{34}N_4RuP_2F_6$ (883.2): C, 58.14; H, 3.86; N, 6.31. Found: C, 58.11; H, 3.90; N, 6.59%. ^{1}H NMR (400 MHz, $CDCl_3$, δ) 9.50 (d, 1H), 8.75 (d, 1H), 8.72 (d, 1H), 8.21 (s, 1H), 8.14 (td,1H), 7.57 (td, 1H), 7.37 (td, 1H), 7.30–7.20 (m, 20H),7.14 (td, 1H) 6.78 (d, 1H), 4.83 (s, 5H, C_5H_5) ppm. ^{31}P{1H} = 46.12 ppm. ESI-MS (*m*/*z*): 743.5 (100%) $[M-PF_6]^+$. IR (KBr, cm^{-1}): $\nu_{(P-F)}$ 842s; 527m.

3.3.2. $[(\eta^5\text{-}C_5Me_5)Ru(L^{ph})(PPh_3)]PF_6$ (**7**)

Orange color, yield 68 mg (60%): Anal. Calc. for $C_{48}H_{44}N_4RuP_2F_6$ (953.38): C, 60.16; H, 4.63; N, 5.85. Found: C, 60.11; H, 4.69; N, 5.74%. ^{1}H NMR (400 MHz, $CDCl_3$, 25 °C): δ = 9.07 (d, 1H), 8.89 (d, 1H), 8.81 (td, 1H), 8.25 (s, 1H), 8.17 (td, 1H), 7.51–7.12 (m, 23H), 6.76 (d, 1H), 4.90 (s, 5H, C_5Me_5) ppm. ^{31}P{1H} = 45.25 ppm. ESI-MS (*m*/*z*): 818.1 (100%) $[M-PF_6]^+$. IR (KBr, cm^{-1}): $\nu_{(PF)}$ 844s; 527m.

3.3.3. $[(\eta^5\text{-}C_9H_7)Ru(L^{ph})(PPh_3)]PF_6$ (**8**)

Yellowish brown color, yield 70 mg (83%): Anal. Calc. for $C_{47}H_{36}N_4RuP_2F_6$ (933.3): C, 60.16; H, 3.87; N, 5.97. Found: C, 60.11; H, 3.89; N, 5.99%. ^{1}H NMR (400 MHz, $CDCl_3$, 25 °C):

δ = 9.68 (d, 1H), 8.76 (d, 1H), 8.69 (d, 1H), 8.20 (s, 1H), 8.12 (td, 2H), 7.94 (td, 2H) 7.63 (td, 1H), 7.22–7.55 (m, 24H, 4Ph), 4.87(t, 1H), 4.71 (d, 2H) ppm. $^{31}P\{1H\}$ = 48.42 ppm. ESI-MS (*m*/*z*): 789.4 (100%) $[M-PF_6]^+$. IR (KBr, cm^{-1}): $\nu_{(P-F)}$ 841s; 548m.

3.4. Single-crystal X-ray structure analyses

X-ray quality crystals of the complex **2**. $CHCl_3$ were obtained by the slow diffusion of diethyl ether into a chloroform solution of **2**, while the crystals of **4** and **6** were obtained from slow evaporation of their reaction mixtures. The data were measured using a Bruker SMART CCD diffractometer using Mo Kα graphite monochromated radiation (α = 0.71073 Å). The structures were solved by direct methods using the program SHELXS-97 [63]. Refinement and all further calculations were carried out using SHELXL-97 [64]. Hydrogen atoms were included at the calculated positions and treated as riding atoms using the SHELXL default parameters. The non-H atoms were refined anisotropically, using weighted full-matrix least-squares on F^2. Crystallographic details are summarized in Table 2. Figs. 5–7 were drawn with ORTEP [65], representing the structures of complexes **2**, **4** and **6**, respectively.

3.5. Theoretical calculations

Density functional theory (DFT) [66] calculations were undertaken for the ligands L and L^{ph} as well as for the complexes $[(\eta^6\text{-}p\text{-}^iPrC_6H_4Me)Ru(L^{ph})Cl]^+$, $[(\eta^5\text{-}C_5Me_5)Rh(L^{ph})Cl]^+$, $[(\eta^5\text{-}C_5Me_5)Ir(L^{ph})Cl]^+$, $[\eta^5\text{-}C_5H_5)Ru(L^{ph})(PPh_3)]^+$ in both the binding modes (*type-A* and *type-B*). Full geometry optimization was carried out with the use of the B3LYP [Becke three-parameter exchange functional (B3) and the Lee–Yang–Parr correlation functional (LYP)] method [67,68] together with the 6-31+G** and LanL2DZ [69–71] basis sets for ligands and for complexes, respectively. Staring atomic coordinates for the cationic complexes (**2**, **4** and **6)** were taken from the single-crystal X-ray structures. All computations were performed with the GAUSSIAN 03 package [72]. Frequency calculations were performed to determine whether the optimized geometries were minima on the potential energy surface.

Acknowledgements

K.M. Rao gratefully acknowledges the Department of Science and Technology, New Delhi, for financial support (Sanction Order No. SR/S1/IC-11/2004). We thank the Sophisticated Instruments Facility, Indian Institute of Science, Bangalore, for providing the NMR facility. Thanks are due to Professor R.H. Duncan Lyngdoh for help in preparing this manuscript.

Appendix A. Supplementary data

CCDC 739572, 739570 and 739571 contain the supplementary crystallographic data for **2**·$CHCl_3$, **4** and **6**. These data can be obtained free of charge from The Cambridge Crystallographic Data Centre via www.ccdc.cam.ac.uk/data_request/cif. Supplementary data associated with this article can be found, in the online version, at doi:10.1016/j.jorganchem.2009.12.004.

References

[1] M.H. Keefe, K.D. Benkstein, J.T. Hupp, Coord. Chem. Rev. 205 (2008) 201–228.
[2] D.S. Tyson, C.R. Luman, X. Zhou, F.N. Castellano, Inorg. Chem. 40 (2001) 4063–4071.
[3] J.F. Endicott, H.B. Schlegel, Md.J. Uddin, D.S. Seniveratne, Coord. Chem. Rev. 229 (2002) 95–106.
[4] W.R. Browne, R. Hage, J.G. Vos, Coord. Chem. Rev. 250 (2006) 1653–1668.
[5] M.T. Indelli, C. Chiorboli, F. Scandola, Top. Curr. Chem. 80 (2007) 215.
[6] M. Yanagida, L.P. Singh, K. Sayama, K. Hara, R. Katoh, A. Islam, H. Sugihara, H. Arakawa, M.K. Nazeeruddin, M. Grätzel, J. Chem. Soc., Dalton Trans. 16 (2000) 2817–2822.
[7] P.R. Ashton, R. Ballardini, V. Balzani, A. Credi, K.R. Dress, E. Ishow, C.J. Clevelaan, O. Kosian, J.A. Preece, N. Spencer, J.F. Stoddart, M. Venturi, S. Wenger, Chem. Eur. J. 6 (2008) 3558–3574.
[8] F. Hanasaka, K.-I. Fujita, R. Yamaguchi, Organometallics 24 (2005) 3422–3433.
[9] M.S. El-Shahawi, A.F. Shoair, Spectrochim. Acta, Part A 60 (2004) 121–127.
[10] R. Noyori, S. Hashigushi, Acc. Chem. Res. 30 (1997) 97–102. and reference therein.
[11] S.-I. Murahashi, H. Takaya, T. Naota, Pure Appl. Chem. 74 (2002) 19–23.
[12] U.J. Jauregui-Haja, M. Dessoudeix, P. Kalck, M. Wilhelm, H. Delmas, Catal. Today 66 (2001) 297.
[13] C.A. Sandoval, T. Ohkuma, N. Utsumi, K. Tsutsumi, K. Murata, R. Noyori, Chem. Asian J. 1–2 (2006) 102–110.
[14] P.J. Dyson, G. Sava, Dalton Trans. (2006) 1929–1933.
[15] W.H. Ang, P.J. Dyson, Eur. J. Inorg. Chem. (2006) 4003–4018.
[16] A.F.A. Peacock, A. Habtemariam, R. Fernandez, V. Walland, F.P.A. Fabbiani, S. Parsons, R.E. Aird, D.I. Jodrell, P.J. Sadler, J. Am. Chem. Soc. 128 (2006) 1739–1748.
[17] A. Habtemariam, M. Melchart, R. Fernandez, S. Parsons, I.D.H. Oswald, A. Parkin, F.P.A. Fabbiani, J.E. Davidson, A. Dawson, R.E. Aird, D.I. Jodrell, P.J. Sadler, J. Med. Chem. 49 (2006) 6858–6868.
[18] M. Melchart, A. Habtemariam, O. Novakova, S.A. Moggach, F.P.A. Fabbiani, S. Parsons, V. Brabec, P.J. Sadler, Inorg. Chem. 46 (2007) 8950–8962.
[19] C. Scolaro, A. Bergamo, L. Brescacin, R. Delfino, M. Cocchietto, G. Laurenczy, T.J. Geldbach, G. Sava, P.J. Dyson, J. Med. Chem. 48 (2005) 4161–4171.
[20] E. Hilllard, A. Vessieres, F. Le Bideau, D. Plazuk, D. Spera, M. Huche, G. Jaouen, Chem. Med. Chem. 1 (2006) 551–559.
[21] M. Auzias, B. Therrien, G. Süess-Fink, P.P. Štěpnička, W.H. Ang, P.J. Dyson, Inorg. Chem. 47 (2008) 578–583.
[22] M.A. Scharwitz, I. Ott, Y. Geldmacher, R. Gust, W.S. Sheldrick, J. Organomet. Chem. 693 (2008) 2299–2309.
[23] S.K. Singh, S. Joshi, A.R. Singh, J.K. Saxena, D.S. Pandey, Inorg. Chem. 46 (2007) 10869–10876.
[24] M. Haga, M.M. Ali, H. Maegawa, K. Nozaki, A. Yoshimura, T. Ohno, Coord. Chem. Rev. 94 (1994) 99–118.
[25] M. Haga, M.M. Ali, R. Arakava, Angew. Chem. Int., Ed. Engl. 35 (1996) 76–78.
[26] S. Baitalik, U. Florke, K. Nag, Inorg. Chem. 38 (1999) 3296–3308.
[27] N. Gupta, N. Grover, G.A. Neyhart, P. Singh, H.H. Thorp, Inorg. Chem. 32 (1993) 310–316.
[28] B.L. Schottel, H.T. Chifotides, M. Shatruk, A. Chouai, L.M. Pérez, J. Bacsa, K.R. Dunbar, J. Am. Chem. Soc. 128 (2006) 5895–5902.
[29] P. Ceroni, F. Paolucci, S. Roffia, S. Serroni, S. Campagna, A.J. Bard, Inorg. Chem. 37 (1998) 2829–2832.
[30] A.K.V. Kasack, R. Reinhardt, S. Torsten, T. Scheiring, S. Zalis, J. Fiedler, W. Kaim, Dalton Trans. (1999) 575–582.
[31] N. Komatsuzaki, R. Katoh, Y. Himeda, H. Sugihara, H. Arakawa, K. Kasuga, J. Chem. Soc., Dalton Trans. (2000) 2045–2053.
[32] C. Metcalfe, S. Spey, J.A. Thomas, Dalton Trans. (2002) 4732–4739.
[33] P.A. Anderson, F.R. Keene, T.J. Meyer, J.A. Moss, G.F. Strouse, J.A. Treadway, Dalton Trans. (2002) 3820–3831.
[34] E.C. Constable, C.E. Housecroft, M. Neuburger, S. Reymann, S. Schaffner, Eur. J. Org. Chem. (2008) 1597–1607.
[35] E.C. Constable, C.E. Housecroft, M. Neuburger, S. Reymann, S. Schaffner, Eur. J. Inorg. Chem. (2008) 3540–3548.
[36] E.C. Constable, C.E. Housecroft, B.M. Kariuki, N. Kelly, C.B. Smith, Inorg. Chem. Commun. 5 (2002) 199–202.
[37] E.C. Constable, C.E. Housecroft, B.M. Kariuki, M. Neuburger, C.B. Smith, Aust. J. Chem. 56 (2003) 653–655.
[38] N. Singh, D.S. Pandey, J. Organomet. Chem. 689 (2004) 1821–1834.
[39] S. Ghumaan, B. Sarkar, S. Patra, K. Parimal, J.V. Slageren, J. Fiedler, W. Kaim, G.K. Lahiri, J. Chem. Soc., Dalton Trans. (2005) 706–712.
[40] Z. Deng, H.-W. Tseng, R. Zong, D. Wang, R.P. Thummel, Inorg. Chem. 47 (2008) 1835–1848.
[41] P. Govindaswamy, Y.A. Mozharivskyj, K.M. Rao, J. Organomet. Chem. 689 (2004) 3265–3274.
[42] P. Govindaswamy, P.J. Carroll, Y.A. Mozharivskyj, K.M. Rao, J. Organomet. Chem. 690 (2005) 885–894.
[43] A. Singh, N. Singh, D.S. Pandey, J. Orgnomet. Chem. 642 (2002) 48–57.
[44] R. Dorta, L. Konstantinovski, L.J.W. Shimon, Y. Ben-David, D. Milstein, Eur. J. Inorg. Chem. (2003) 70–76.
[45] K.T. Prasad, B. Therrien, K.M. Rao, J. Organomet. Chem. 693 (2008) 3049–3056.
[46] B. Therrien, C. Said-Mohamed, G. Suss-Fink, Inorg. Chim. Acta 361 (2008) 2601–2608.
[47] R. Lalrempuia, K.M. Rao, Polyhedron 22 (2003) 3155–3160.
[48] P. Govindaswamy, Y.A. Mozharivskyj, K.M. Rao, Polyhedron 24 (2005) 1710–1716.
[49] K. Pachhunga, B. Therrien, K.A. Kreisel, G.P.A. Yap, K.M. Rao, Polyhedron 26 (2007) 3638–3644.
[50] J.G. Małecki, R. Kruszynski, M. Jaworska, P. Lodowski, Z. Mazurak, J. Organomet. Chem. 693 (2008) 1096–1108.
[51] E. Binamira-Soriaga, N.L. Keder, W.C. Kaska, Inorg. Chem. 29 (1990) 3167–3171.
[52] C.S. Araújo, M.G.B. Drew, V. Félix, L. Jack, J. Madureira, M. Newell, S. Roche, T.M. Santos, J.A. Thomas, L. Yellowlees, Inorg. Chem. 41 (2002) 2250–2259.

[53] H. Deng, J. Li, K.C. Zheng, Y. Yang, H. Chao, L.N. Ji, Inorg. Chim. Acta 358 (2005) 3430–3440.
[54] M.A. Bennett, T.N. Huang, T.W. Matheson, A.K. Smith, Inorg. Synth. 21 (1982) 74–81.
[55] M.A. Bennett, T.W. Matheson, G.B. Robertson, A.K. Smith, P.A. Tucker, Inorg. Chem. 19 (1980) 1014–1021.
[56] M.A. Bennett, A.K. Smith, J. Chem. Soc., Dalton Trans. (1974) 233–241.
[57] J.W. Kang, K. Moseley, P.M. Maitlis, J. Am. Chem. Soc. 91 (1969) 5970–5977.
[58] R.G. Ball, W.A.G. Graham, D.M. Heinekey, J.K. Hoyano, A.D. McMaster, B.M. Mattson, S.T. Michel, Inorg. Chem. 29 (1990) 2023–2025.
[59] C. White, A. Yates, P.M. Maitlis, Inorg. Synth. 29 (1992) 228.
[60] M.I. Bruce, N.J. Windsor, Aust. J. Chem. 30 (1977) 1601–1604.
[61] G. Consiglio, F. Morandini, Chem. Rev. 87 (1987) 761–778.
[62] W.A. Butte, F. Case, J. Org. Chem. 26 (1961) 4690–4692.
[63] G.M. Sheldrick, Acta Crystallogr., Sect.A 46 (1990) 467–473.
[64] G.M. Sheldrich, SHELXS-97 and SHELXL-97, University of Göttingen, Göttingen, Germany, 1999.
[65] L.J. Farrugia, J. Appl. Crystallogr. 30 (1997) 565–566.
[66] R.G. Parr, W. Yang, Density Functional Theory of Atoms and Molecules, Oxford University Press, New York, 1989.
[67] A.D. Becke, J. Chem. Phys. 98 (1993) 5648–5652.
[68] C. Lee, W. Yang, R.G. Parr, Phys. Rev. B 37 (1988) 785–789.
[69] A.D. Becke, J. Chem. Phys. 98 (1993) 1372.
[70] A. Gorling, Phys. Rev. A 54 (1996) 3912–3915.
[71] L. Tan, S. Zhang, X. Liu, Y. Chen, X. Liu, J. Organomet. Chem. 693 (2008) 3387–3395.
[72] M.J. Frisch, G.W. Trucks, H.B. Schlegel, G.E. Scuseria, M.A. Robb, J.R. Cheeseman, J.A. Montgomery, T. Vreven, K.N. Kudin, J.C. Burant, J.M. Millam, S.S. Iyengar, J. Tomasi, V. Barone, B. Mennucci, M. Cossi, G. Scalmani, N. Rega, G.H. Petersson, H. Nakatsuji, M. Hada, M. Ehara, K. Toyota, R. Fukuda, J. Hasegawa, M. Ishida, T. Nakajima, Y. Honda, O. Kitao, H. Nakai, M. Klene, X. Li, J.E. Knox, H.P. Hratchian, J.B. Cross, C. Adamo, J. Jaramillo, R. Gomperts, R.E. Stratmann, O. Yazyev, A.J. Austin, R. Cammi, C. Pomelli, J.W. Ochterski, P.Y. Ayala, K. Morokuma, G.A. Voth, P. Salvador, J.J. Dannenberg, V.G. Zakrzewski, S. Dapprich, A.D. Daniels, M.C. Strain, O. Farkas, D.K. Malick, A.D. Rabuck, K. Raghavachari, J.B. Foresman, J.V. Ortiz, Q. Cui, A.G. Baboul, S. Clifford, J. Cioslowski, B.B. Stefanov, G. Liu, A. Liashenko, P. Piskorz, I. Komaromi, R.L. Martin, D.J. Fox, T. Keith, M.A. Al-Laham, C.Y. Peng, A. Nanayakkara, M. Challacombe, P.M.W. Gill, B. Johnson, W. Chen, M.W. Wong, C. Gonzalez, J.A. Pople, GAUSSIAN 03, Revision E.01, Gaussian, Inc., Pittsburgh, PA, 2003.